Chemical Science

ROYAL SOCIETY OF CHEMISTRY

EDGE ARTICLE

View Article Online
View Journal | View Issue

Cite this: *Chem. Sci.*, 2024, **15**, 10101

All publication charges for this article have been paid for by the Royal Society of Chemistry

Received 14th April 2024
Accepted 20th May 2024

DOI: 10.1039/d4sc02459a

rsc.li/chemical-science

Difluorenoheteroles: topological control of π conjugation in diradicaloids and mixed-valence radical ions†

Bibek Prajapati,[a] Tendai Kwenda,[a] Tadeusz Lis,[a] Piotr J. Chmielewski,[a] Carlos J. Gómez-García,[b] Marcin A. Majewski[a] and Marcin Stępień*[a]

Two families of difluorenoheterole diradicaloids were synthesized, featuring isomeric ring systems with distinct conjugation topologies. The two types of difluorenoheteroles contain, respectively, a Chichibabin-like motif (**CH**) and a newly introduced heteroatom-linked triphenylmethyl dyad (**TD**-X). Combined experimental and theoretical investigations show that the **TD**-X systems have reduced quinoidal character but the interaction between formal spin centers is sufficiently strong to ensure a singlet ground state. The singlet–triplet energy gaps in the **TD**-X difluorenoheteroles are strongly affected by the heterocyclic ring, with values of −4.3 and −0.7 kcal mol^{-1} determined for the pyrrole- and thiophene-containing analogues, respectively. In cyclic voltammetry experiments, the **TD**-X systems show diminished energy gaps and superior reversibility in comparison with their **CH** counterparts. The radical anions and cations obtained from these diradicaloids show extremely red-shifted bands, occasionally with λ_{max} > 3500 nm. Computational studies show that some of these ions adopt distonic structures and may be characterized as class-II mixed-valence species.

Introduction

Chichibabin's hydrocarbon,[1] one of the oldest known diradicaloids (**CH**, Chart 1), can be viewed as a pair of triphenylmethyl (**TPM**) radicals conjoined at *para*-phenyl positions. Such a topology leads to a relatively strong interaction between the two spin centers, resulting in a singlet ground state.[2] However, this interaction alone is insufficient to ensure good ambient stability, unless additional modifications, such as electron-withdrawing groups,[3] are introduced. In particular, the chemical robustness of Chichibabin's hydrocarbon can be enhanced by ring fusion and peripheral substitution, as illustrated by the recently reported derivatives of **CH**, such as 5,10-dimesityldiindeno[1,2-*a*:2′,1′-*i*]phenanthrene (**DIPh**),[4] its heterocyclic analogues **DFFu**,[5] **DFPy** and **DFTh**,[6] and some coronoid oligoradicaloid structures.[7–9] These systems exemplify the use of indeno fusion[10–12] as a strategy for elaborating stable di- and oligoradicaloids, which are of interest as organic semiconductors,[6,13,14] redox-active systems,[15] ion receptors,[8] and chiral materials.[16,17] Heterocycle fusion, showcased by **DFFu**,

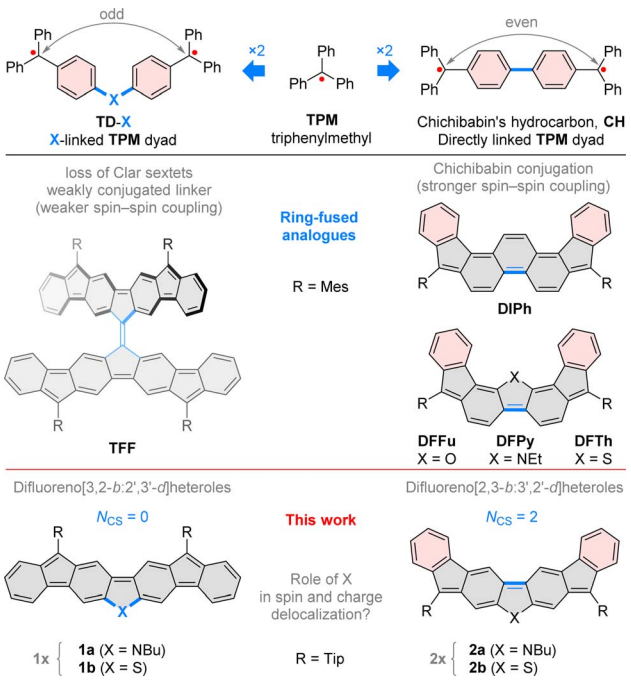

Chart 1 Difluorenoheteroles and the influence of ring fusion on spin–spin interactions in indeno-fused oligoradicals. Mes, mesityl; Tip, 2,4,6-tri(isopropyl)phenyl. NCS, clar-sextet count.

[a]*Wydział Chemii, Uniwersytet Wrocławski, ul. F. Joliot-Curie 14, 50-383, Wrocław, Poland. E-mail: marcin.stepien@uwr.edu.pl*

[b]*Departamento de Química Inorgánica, Universidad de Valencia, Dr Moliner 50, 46100 Burjasot, Spain*

† Electronic supplementary information (ESI) available. CCDC 2302632–2302634. For ESI and crystallographic data in CIF or other electronic format see DOI: https://doi.org/10.1039/d4sc02459a

DFPy and **DFTh**, is a complementary approach to effectively stabilizing open-shell organics, with diverse recent examples documented in the literature.[18–23]

The spin–spin interaction in such diradicaloids can be engineered by modifying the topology of the π-system. A simple alteration of the original Chichibabin structure involves insertion of a monoatomic linker X, potentially bearing an additional substituent, in between the two constituent **TPM** units (**TD**-X, Chart 1). An early attempt to obtain such a diradical with X = O (**TD**-O), produced a transiently paramagnetic species,[24–27] which apparently oligomerized on standing. N-linked diradicals **TD**-NR (R = H, aryl)[27,28] can be made more stable by chlorination of aryl rings,[28] however communication between radical centers is weakened by the nonplanarity of the π system.

Rajca's trimethylenemethane benzologue[29] and Wu's fluorenyl dendrons[30] offer examples of C-linked oligoradicaloids based on the **TD**-X conjugation type, displaying respectively ferromagnetic and antiferromagnetic coupling between spin centers. The recently reported tetrafluorenofulvalene (**TFF**, Chart 1), which can be seen as a dyad of **TD**-C moieties, features a complex relationship between its electronic state and the center alkene bond strength.[31] **TFF** differs from the former two systems in that a fully planarized conjugation pathway exists between the two formal spin centers in each of the **TD**-C subunits.

Our investigations of **TFF** suggested that the extension of the conjugation pathway introduced by the X linker may produce weakly coupled diradicals with unique spin and redox characteristics. In particular, we considered two isomeric difluorenoheterole motifs **1a–b** (labeled jointly **1x**) and **2a–b** (**2x**, Chart 1), in which the seemingly similar ring fusion patterns produce very different spin-coupling topologies. While **2x** can be analyzed as **CH**-like systems with even-electron coupling pathways, in **1x**, the shortest path between formal spin centers contains an odd number of atoms and includes the heteroatom linker X. In addition, the closed-shell formulae of **1x** contain no Clar sextets ($N_{CS} = 0$), whereas two sextets are present in **2x**, similarly as in other diindeno analogues of **CH**. While **1x** can be expected to be more weakly coupled that their **2x** isomers, the involvement of X bridges in conjugation is far less evident. To study the latter effect, we focused on difluorenopyrroles (**1a** and **2a**, X = NR) and difluorenothiophenes (**1b** and **2b**, X = S). Our choice was motivated by the electron-rich character of both heterocycles, which was thought to facilitate exploration of positively charged states, and the expected difference in π-conjugation between a second- and third-row heteroatom centers.

The four difluorenoheteroles **1a**, **1b**, **2a**, and **2b** were obtained using a three-step procedure summarized in Scheme 1. Syntheses of the requisite dibromodialdehydes **3a**, **3b**, **6a**,[32] and **6b** were designed by taking into account intrinsic reactivities of dibenzothiophene and carbazole (see the ESI†). Subsequently, the seven-ring framework of each difluorenoheterole was constructed by double Suzuki coupling followed by Grignard addition of the bulky 2,4,6-tri(isopropyl)phenyl (Tip) group, and electrophilic pentannulation. In each case, formyl groups were strategically placed at the heterocyclic core of **4a–b** and **7a–b**, to ensure complete regioselectivity of ring closures in step b, which could not be achieved with *ortho*-formylphenyl substituents. Ultimately, the resulting dihydro precursors **5a**, **5b**, **8a**, and **8b**, were deprotonated using potassium *tert*-butoxide, and conveniently oxidized with copper(I) iodide. The desired diradicaloids were obtained in high yield and isolated as crystalline solids. **1a** and **1b** were relatively unstable, and had to be handled and stored in an inert atmosphere. Their isomeric congeners had better stability: refrigerated solid samples **2a** and **2b** could be stored in air, but the corresponding solutions would gradually decompose over the course of several hours. In spite of structural similarities, the four difluorenoheteroles showed markedly different colors in the solid state, being respectively green (**1a**), brown (**1b**), red (**2a**), and pink (**2b**).

Single crystals of the four difluorenoheteroles were grown using vapor diffusion under strictly inert conditions (see the ESI†). X-ray diffraction analyses performed on these crystals confirmed the structures of all diradicaloids, except that, in the case of **1b**, the quality of diffraction data was insufficient for complete refinement. As a complementary source of structural data we used DFT calculations, which were performed for the

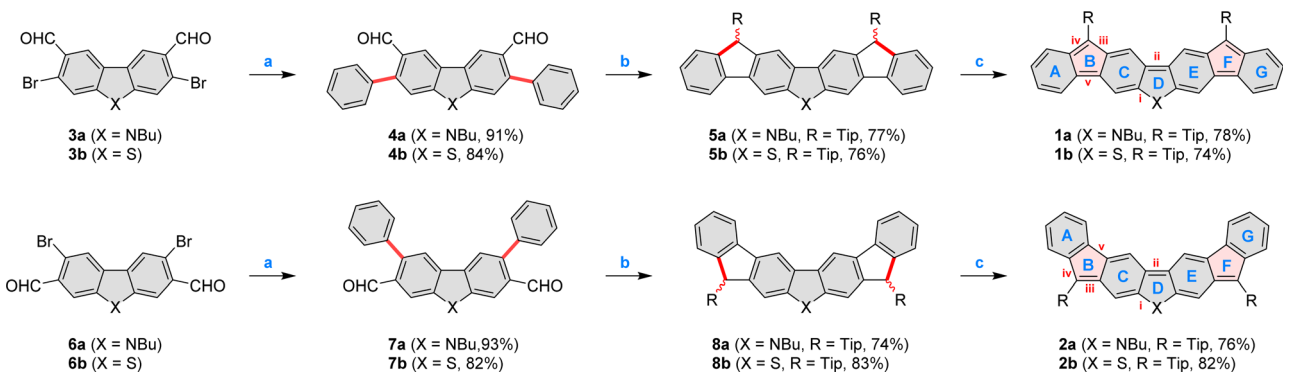

Scheme 1 Synthesis of difluorenoheteroles **1x** and **2x**. Reagents and conditions: (a) phenylboronic acid (2.5 equiv.), $Pd(PPh_3)_4$ (0.1 equiv.), Na_2CO_3 (8.0 equiv.), dioxane, H_2O, 24 h; (b) (1) TipMgBr (0.5 M solution in THF, 6.0 equiv.), THF, overnight. (2) $BF_3 \cdot Et_2O$, DCM, 15 min; (c) (1) *t*-BuOK (2 M in 2-MeTHF, 6.0 equiv), THF, (2) CuI (4.0 equiv.), 15 min. For the synthesis of the new dialdehydes **3a**, **3b**, and **6b**, see the ESI.† New bonds and modified rings, are shaded in red. Labelling of key rings (blue) and bonds (red) is given for **1x** and **2x**.

substituent-free systems **1a**′, **1b**′, **2a**′, and **2b**′, for all of the relevant spin states and oxidation levels. Experimental and theoretical geometries of each difluorenoheterole are very similar (Fig. 1, and ESI†): each system is predicted to be perfectly planar in the gas phase (C_{2v} point symmetry), and the planarity is largely preserved in the solid state. No π stacking interactions were however observed in the crystals, apparently because of the steric hindrance introduced by the bulky Tip groups.

The balance between quinoidal and radicaloid contributions can be assessed using relative lengths of bonds **iii** contained in the outer five-membered rings (Scheme 1). In **2a** and **2b**, these distances are significantly longer than formal double bonds but they are nevertheless shorter than the corresponding **iv** distances (Fig. 1). The difference between **iii** and **iv** distances becomes smaller in the **1x** series, implying a relatively higher diradicaloid character. Structural variations within the center heterole rings reveal further differences: the center bond **ii** in **2x** is somewhat shorter than the corresponding distance in **1x**, in line with the Chichibabin-like quinoidal contribution. Conversely, slight shortening of the C–X bonds (**i**) in the **1x** systems may be thought to indicate involvement of heteroatoms in π-conjugation between the spin centers.

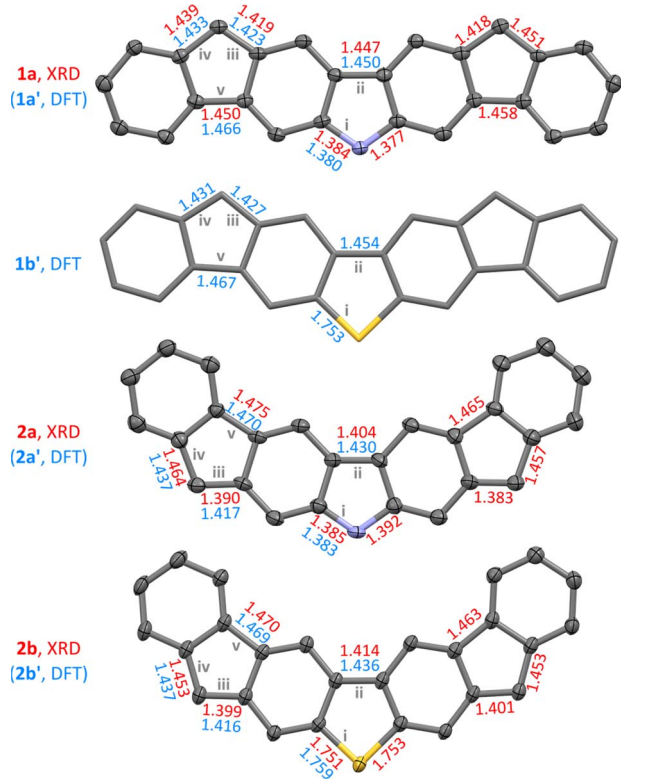

Fig. 1 Molecular structures and selected bond distances (Å) of difluorenoheteroles, as obtained from single-crystal X-ray diffraction analyses (XRD, red labels) and DFT calculations (GD3BJ-CAM-B3LYP/6-31G(d,p), broken-symmetry singlets, **1x**′ and **2x**′ structures, with R = H, blue labels). For **1a**, **2a**, and **2b**, XRD geometries are shown, with solvent molecules, hydrogen atoms, and substituents removed for clarity (thermal ellipsoids at the 50% probability level). C–C bond precision of these XRD geometries is 0.0038 Å (**1a**), 0.0084 Å (**2a**), and 0.0029 Å (**2b**), respectively. A DFT-optimized geometry is shown for **1b**′ (R = H). Interatomic distances are given for bonds **i**–**v**, as defined in Scheme 1.

All difluorenoheteroles show distinct room-temperature magnetism, consistent with non-negligible populations of the respective triplet states. The paramagnetic nature of solution samples was inferred from variable-temperature ^{1}H NMR spectroscopy (Fig. S46–S49†). Specifically, **2a** and **2b** yielded sharp spectra at 200 K, but the linewidths would progressively increase when the samples were heated to room temperature. In contrast, **1a** produced a broadened spectrum even at 160 K, whereas **1b** remained NMR-silent from room temperature down to 180 K. The relative triplet populations cannot however be inferred from these observations since in the fast exchange limit the paramagnetic broadening of NMR lines depend additionally on hyperfine coupling constants and exchange rates,[33] which may differ among the species being compared. The presence of triplets was verified for compounds **1a**, **2a**, and **2b**, which showed characteristic zero-field splitting patterns in their ESR spectra (Table 1, Fig. S50 and S51†). For **1b**, no triplet species was observed, possibly because of unfavorable relaxation effects. However, in SQUID magnetometry, all four systems revealed temperature dependencies consistent with a singlet ground state and a thermally accessible triplet. Interestingly, the ΔE_{ST} gap estimated for **1a** using the Bleaney–Bowers model (−4.3(1) kcal mol^{-1}) has a larger absolute value than the corresponding value obtained for **1b** (−0.71(1) kcal mol^{-1}). In comparison, gaps of −1.46(1) and −1.42(1) kcal mol^{-1} were determined for **2a** and **2b**, respectively. The latter two gaps have much smaller absolute values than those of the corresponding isomers, **DFPy** and **DFTh** (−5.0 and −4.3 kcal mol^{-1}, respectively).[6] These results show that the energetics of spin alignment in difluorenoheterole diradicaloids depend in a complex way on the topology of the π system and the identity of the heteroatom.

In electrochemical experiments, all difluorenoheteroles, **1a**, **1b**, **2a**, and **2b**, exhibited two one-electron oxidations (Fig. 2). In particular, the first oxidation is fully reversible in all systems, and occurs at relatively low potentials. Pyrroles are easier to oxidize than the corresponding thiophenes, indicating a more electron-donating character of the NBu fragment in comparison with the sulfur center. The **1x** series is more easily oxidized than the **2x** series, with **1a** displaying a particularly low E_{ox1} potential of −0.26 V *vs.* Fc^+/Fc. This finding is consistent with better delocalization of the positive charge in the **1x** series (*vide infra*). The second oxidation showed very good reversibility in the **1x** series, whereas non-reversible processes were observed for **2a** and, especially **2b**. Two reversible one-electron reduction events were observed for each system, with less variable redox potentials than observed for the oxidations. Overall, the **1x** systems show smaller electrochemical energy gaps than their **2x** counterparts, with the smallest $\Delta E = 1.21$ found for **1a**. Interestingly, **2a** and **2b** are somewhat more electron-rich than their isomers, **DFPy** and **DFTh**,[6] respectively, featuring E_{ox} values lower by *ca.* 0.2 eV, and somewhat reduced electrochemical gaps.

The absorption spectra of **2a** and **2b** each contain an intense maximum at 574 nm and 565 nm, respectively, followed by a group of weaker lower-energy features above 700 nm (navy-blue traces, Fig. 3). These spectra qualitatively resemble those

Table 1 Experimental and theoretical characteristics of neutral difluorenoheteroles[a]

Species	ΔE_{ST}[b] (kcal mol^{-1})	zfs[e]	^{1}H NMR	Species	ΔE_{ST}^{CAM}[b] (kcal mol^{-1})	y_0^{CAM}	y_0^{CAS}	n_U^{CAM}	n_U^{CAS}
1a	−4.3(1)[c] −4.16(10)[d]	D = 109 G E = 16 G	300 K: very broad 160 K: broad	**1a′**	1.21	0.846	0.841	1.800	1.683
1b	−0.71(1)[c] −0.93(3)[d]	[f]	200–300 K: unobservable	**1b′**	0.59	0.914	0.918	1.941	1.835
2a	−1.46(1)[e]	[f]	300 K: broad 200 K: sharp	**2a′**	1.98	0.761	0.694	1.640	1.387
2b	−1.42(1)[c]	D = 83 G	300 K: broad 200 K: sharp	**2b′**	2.45	0.750	0.683	1.624	1.366

[a] y_0 and n_U are, the diradicaloid index and number of unpaired electrons respectively; CAM and CAS denote the respective levels of theory (see text). [b] Singlet–triplet gap. [c] SQUID magnetometry. [d] ESR spectroscopy. [e] Triplet zero field splitting parameters. [f] Splitting not observable.

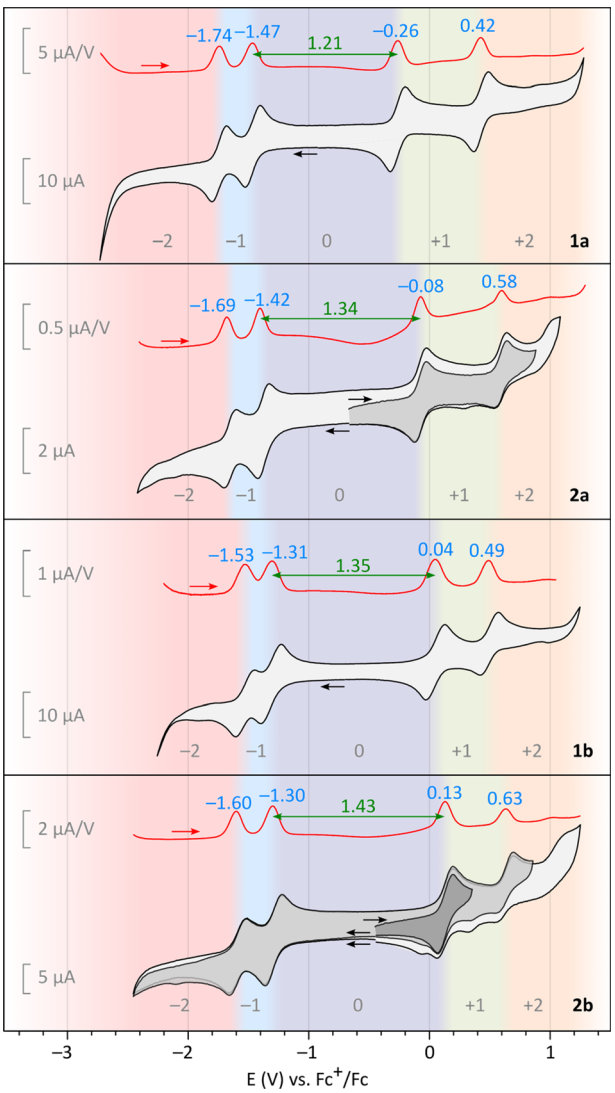

Fig. 2 Cyclic voltammetry (CV, black-gray) and differential pulse voltammetry (DPV, red) obtained for difluorenoheteroles **1x** and **2x** (TBAPF$_6$, dichloromethane, 100 mV s^{-1}). Blue labels indicate positions of maxima in DPV scans. Electrochemical energy gaps, defined as $\Delta E = E_{ox1} - E_{red1}$, are indicated in green. Color shading indicates the oxidation level dominant at a particular potential.

of other **CH**-conjugated diradicaloids **DIPh**,[4] **DFPy**, and **DFTh**,[6] but they feature a much better separation between the visible and NIR absorption ranges. In contrast, in the spectra of **1a** and **1b**, there is no strong feature in the visible region, but the NIR bands have a similar appearance. The apparent optical energy gaps increase in the order **2a** < **1a** < **2b** ∼ **1b**, somewhat different

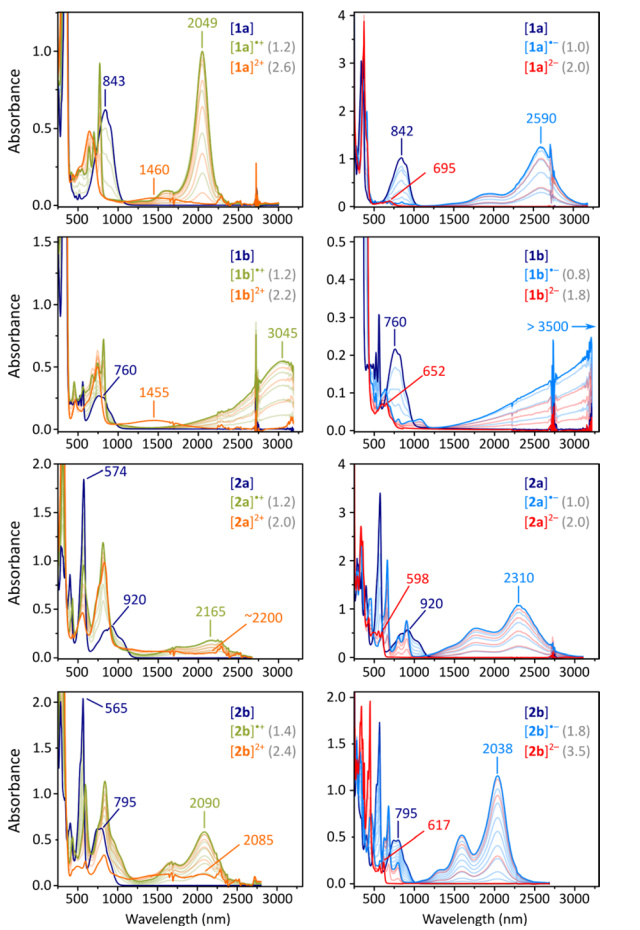

Fig. 3 Titration of difluorenoheteroles **1x** and **2x** with tris(4-bromophenyl)ammoniumyl hexachloroantimonate (BAHA, in dichloromethane, left) and sodium anthracenide (in **THF**, right). Traces corresponding to maximum concentration of +2, +1, 0, −1, and −2 states are colored in orange, olive green, dark blue, light blue, and red, respectively. Values in gray indicate the number of added equivalents.

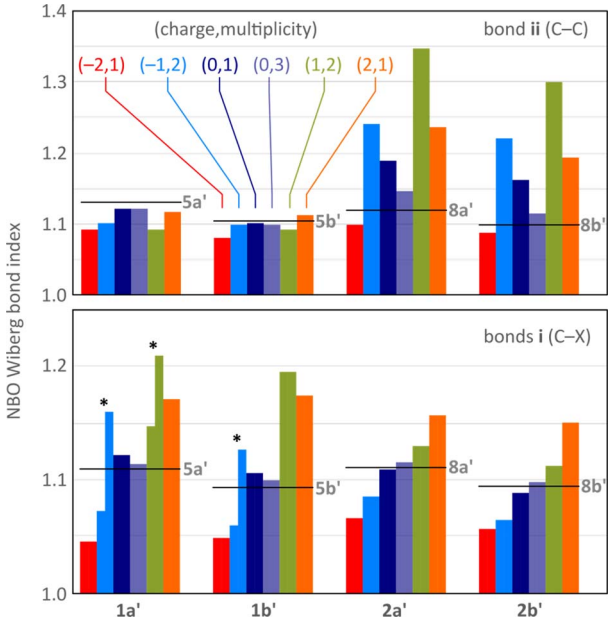

Fig. 4 Evolution of selected Wiberg bond indices as a function of increasing charge calculated for the unsubstituted structures **1a′**, **1b′**, **2a′**, and **2b′** (NBO3/CAM-B3LYP-GD3BJ/6-31G(d,p)). Black horizontal lines indicate reference values obtained for the dihydro reference systems **5a′**, **5b′**, **8a′**, and **8b′**, respectively (Scheme 1, R = H). Bonds **i** and **ii** (defined in Scheme 1) are shown using separate color scales. For the C_s-symmetric structures (denoted with asterisks), *i.e.* $[\mathbf{1a'}]^{\bullet-}$, $[\mathbf{1b'}]^{\bullet-}$, and $[\mathbf{1a'}]^{\bullet+}$, the two **i** bonds have unequal Wiberg indices and are shown with two separate bars.

than observed electrochemically; however, the gaps are again shown to increase on going from pyrrole-to thiophene-containing diradicaloids.

Electrochemically observed redox events were subsequently reproduced in chemical oxidation and reduction experiments (Fig. 3). Each species could be oxidized in two steps using BAHA, yielding the corresponding radical cation and dication. All of the dications (orange traces, Fig. 3) showed relatively weak NIR absorption bands (1000–2500 nm), whereas striking diversity was observed for the radical cations (olive traces). $[\mathbf{2a}]^{\bullet+}$ and $[\mathbf{2b}]^{\bullet+}$ showed qualitatively similar spectra, with the major NIR maxima at 2165 and 2090 nm, respectively. For $[\mathbf{1a}]^{\bullet+}$, a very narrow and intense band was found at 2049 nm, accompanied by a set of sharp features in the 500–800 nm range. Remarkably, the thiophene containing $[\mathbf{2a}]^{\bullet+}$ featured a spectacular shift of its NIR maximum (3045 nm), in opposition to the energy gap relationship established for the neutral states.

Reduction experiments, carried out using sodium anthracenide (NaA) in THF, revealed similar irregularities in the monoanions of our difluorenoheteroles (blue traces, Fig. 3). Radical anions $[\mathbf{2a}]^{\bullet-}$ and $[\mathbf{2b}]^{\bullet-}$, show strong NIR absorptions, reminiscent of those of the respective cations, with energy gaps correlating with those of the neutral states. The NIR band of $[\mathbf{1a}]^{\bullet-}$ already appears at very low energies (2590 nm, 0.48 eV), but a spectacular red shift was observed for the thiophene counterpart $[\mathbf{1b}]^{\bullet-}$. In this species, the NIR absorption extended beyond the measurement limit of our spectrometer (3300 nm), with an expected position of the maximum of $\lambda_{max} > 3500$ nm. Attempts to record an FT-IR spectrum of $[\mathbf{1b}]^{\bullet-}$ met with only partial success, because of the low stability of this species and instrumental difficulties (Fig. S56†). However, available data suggest that the low-energy absorption may extend up to *ca.* 2400 cm^{-1} (*ca.* 4200 nm). Using these values, the energy gap of $[\mathbf{1b}]^{\bullet-}$ can be estimated to lie within the 0.30–0.35 eV range.

By using a larger excess of NaA, the difluorenoheteroles could be cleanly reduced to the corresponding dianions $[\mathbf{1x}]^{2-}$ and $[\mathbf{2x}]^{2-}$ (Fig. 3, red traces). The dianions show much larger energy gaps than the neutral parents or any other ionic states, with somewhat more red-shifted bands found for $[\mathbf{1a}]^{2-}$ and $[\mathbf{1b}]^{2-}$ ($\lambda_{max} = 695$ and 652 nm, respectively). These observations agree with the expected closed-shell character of the difluorenoheterole dianions. The energy gap was similarly diminished in the quadruply charged $[\mathbf{TFF}]^{4-}$,which may be viewed as a "doubled" analogue of the $[\mathbf{1x}]^{2-}$ ions.[31]

Electronic structure features of substituent free difluorenoheteroles were investigated using geometries and densities obtained at the GD3BJ-CAM-B3LYP/6-31G(d,p) level of theory (denoted CAM) along with CAS-SCF(2,2,UNO)/6-31G(d,p) calculations (CAS), carried out on optimized CAM geometries (Table 1). All optimizations yielded flat, C_{2v}-symmetric structures, each containing a pair of equivalent fluorenyl subunits. For the neutral open-shell singlets, diradicaloid indices y_0 (ref. 34) and numbers of unpaired electrons n_U[35] calculated using both methods show the same trend, *i.e.* $^1\mathbf{2a'} \approx {}^1\mathbf{2b'} < {}^1\mathbf{1a'} < {}^1\mathbf{1b'}$. Thus, the influence of the heteroatom on the open-shell character is notably weak in the **2x′** singlets, in line with the predominant Chichibabin-like conjugation along the biphenyl backbone of these molecules. In contrast, the **1x′** singlets reveal a higher open-shell character than their **2x′** counterparts. Most strikingly, there is a significant difference of n_U values between **1b′** and **1a′** (*ca.* 0.15 at the CAS level), which may be seen as an indication that the NR fragment in **1a′** provides a more efficient coupling pathway between radicaloid centers than the S atom in **1b′**.

CAM geometry optimizations carried out for oxidized and reduced forms of **1x′** and **2x′** revealed unexpected symmetry lowering of some states (Fig. S57 and S58†). In most cases, the C_{2v} symmetry of the neutral singlets and triplets was retained in the ions, and structural changes were limited to variations of bond lengths. However, for three radical ions, $[\mathbf{1a'}]^{\bullet-}$, $[\mathbf{1a'}]^{\bullet+}$, and $[\mathbf{1b'}]^{\bullet-}$, C_s symmetric geometries were obtained, with different bonding distances in the two conjoined fluorenyl subunits. Such geometries are consistent with a distonic nature of these radical ions, *i.e.* with preferential localization of the spin and charge on different fluorenyl fragments. The automerization (degenerate rearrangement) of such species would require only a relatively small bond shift, and is expected to have a very low energy barrier. C_{2v}-symmetric stationary points located for $[\mathbf{1a'}]^{\bullet-}$ and $[\mathbf{1a'}]^{\bullet+}$ are transition states according to frequency analyses, but their relative energies are in the 0.1–0.3 kcal mol^{-1} range. The symmetry of global energy minima in the radical ions of **1x** may depend on *e.g.* substitution or solvation and give very soft potentials, and may be represented by the CAM calculation in only an approximate way.[36] For

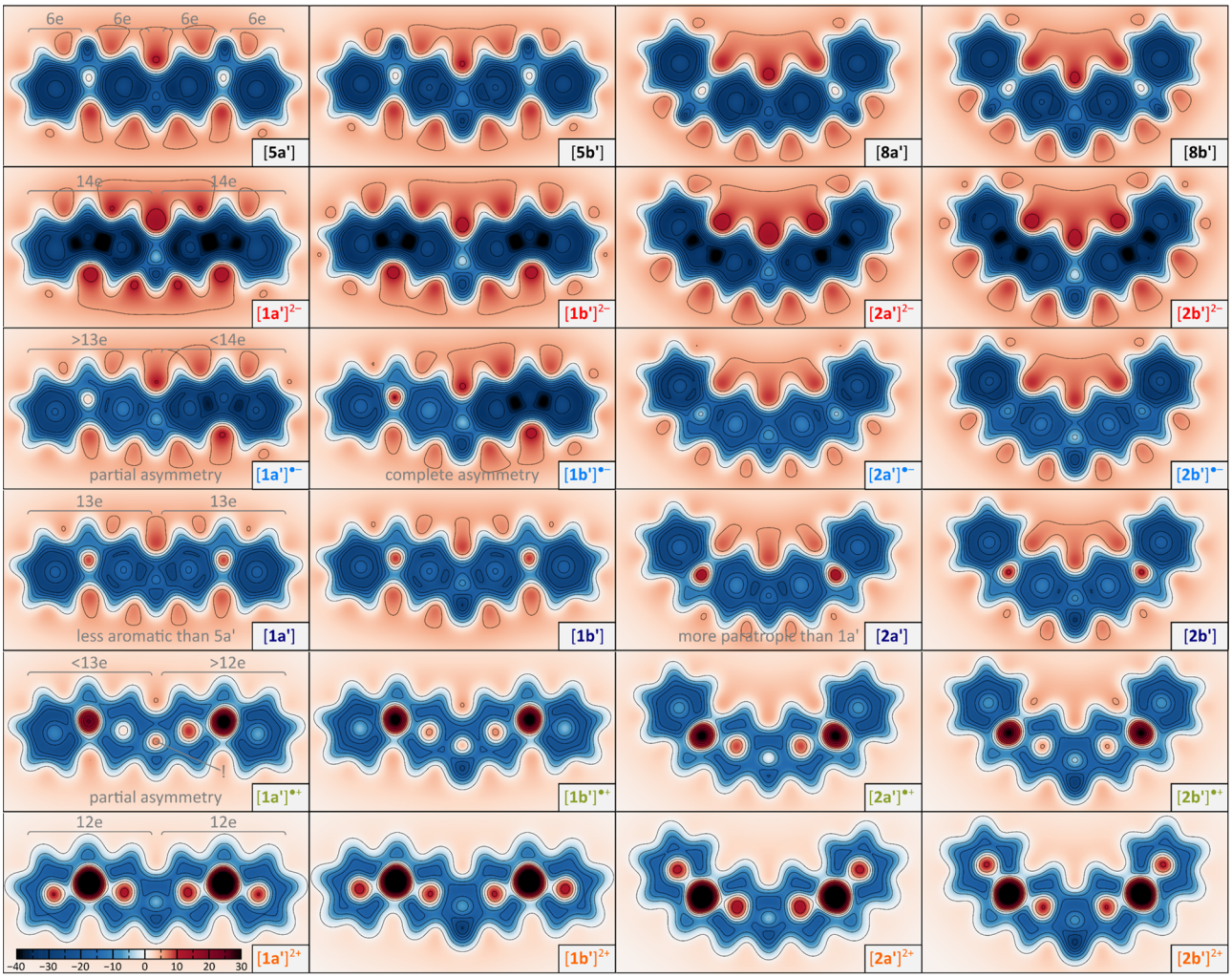

Fig. 5 NICS(1) XY_{zz} scans for the different oxidation levels **1x′** and **2x′** and the dihydro ref. **5x′** and **8x′** (X = S, NH, R = H). The maps show negative values of the *zz* component of the magnetic shielding tensor calculated 1 Å above the mean plane of each molecule at the GIAO/CAM-B3LYP-GD3BJ/6-31G(d,p) level of theory. Electron counts shown for **1a′** and **5a′** show the dominant.

consistency, further discussion corresponds to global minima identified at the CAM level.

In all difluorenoheteroles, coupling between the two halves of the molecule can involve both the C–C pathway (bond **ii**) or the C–X–C pathway (bonds **i**), but the interaction topology differs between the **1x** and **2x** series. Relative contributions of these two pathways as a function of the increasing charge of the system can be inferred from the variations of Wiberg indices[37] obtained for bonds **i** and **ii** in a natural bond orbital analysis[38] (NBO, Fig. 4). The indices of **1a′**, **1b′**, **2a′**, and **2b′** are conveniently compared with values obtained for the corresponding dihydro reference systems, **5a′**, **5b′**, **8a′**, and **8b′**, respectively. All reference systems show relatively weak conjugation between the two fluorene sections of the molecules: the **i** (C–X) and **ii** (C–C) bond indices take relatively low values of 1.09–1.11 and 1.10–1.13, respectively. These indices are essentially independent of the ring fusion pattern (**5x′** *vs.* **8x′**), in line with the absence of cross-conjugation in the dihydro references.

Neutral singlets in the **1x′** series have somewhat stronger **i** bonds than the dihydro ref. **5x′**. This is in contrast with the **2x′** systems, in which the **i** bond indices are lower than in the respective **8x′** references, and may indicate TD-X-like conjugation in **1x′** (as defined in Chart 1). In comparison with the singlets, the **i** and **ii** Wiberg indices in the triplet states ^{3}[**1x′**] and ^{3}[**2x′**] are generally closer to the values observed for dihydro references, implying a weaker interaction between the fluorenyl subunits in the high-spin state. Importantly, in the majority of oxidation levels of **2x′**, the **ii** index is higher than in **8x′**, in line with a Chichibabin-like coupling. Interestingly, the interaction is the strongest in the radical ions [**2x′**]$^+$ and [**2x′**]$^-$, apparently reflecting the involvement of quinoidal conjugation in the delocalization of either the positive or negative charge. The **i** index decreases in the anions of **2x′**, but it becomes higher in the positively charged states, notably in the dications [**2x**]$^{2+}$, a feature attributable to onium-type resonance (*vide infra*). Conversely, the **ii** index is consistently low at all oxidation levels of **1x′**, whereas the **i** index shows a pronounced variation,

becoming particularly high for cationic states. Its values are differentiated in the C_s symmetric states $[\mathbf{1a}']^{\bullet-}$, $[\mathbf{1a}']^{\bullet+}$, and $[\mathbf{1b}']^{\bullet-}$, showing that indeed one of the C–X bonds is stronger than the other.

NICS maps calculated for the difluorenoheteroles (**1x′**, **2x′**) and their dihydro analogues (**5x′**, **8x′**) reveal the relationship between local aromaticity features and the oxidation state (Fig. 5). **5x′** and **8x′** offer a convenient reference picture, displaying the expected aromaticity in all benzenoid rings and in the central heterole unit. Their fully conjugated counterparts **1x′** and **2x′** progress from strong diatropicity to strong paratropicity as their charge is raised from −2 to +2, however, this general trend is superimposed with differences specific to each of the two series. The NICS maps in the neutral singlet states of **1x′** and **2x′** show diminished benzenoid aromaticity relative to the dihydro references, and to a first approximation may be viewed as unions of two 13-electron fluorenyl radicals. However, the greater paratropicity in the **2x′** series, reveals the effect of inter-subunit interactions, and is in line with their stronger quinoidal character of the Chichibabin-like systems. The dianions $[\mathbf{1x}']^{2-}$ and $[\mathbf{2x}']^{2-}$ are magnetically most uniform, and all of them can be viewed as a fused pair of strongly diatropic 14-electron fluorenyl anions. Likewise, the conjugation in $[\mathbf{1x}']^{2+}$ and $[\mathbf{2x}']^{2+}$ can be interpreted in terms of antiaromaticity of the constituent 12-electron fluorenyl cations. Radical anions $[\mathbf{2x}']^{\bullet-}$ reveal shieldings that are intermediate between that of the corresponding dianions and the neutral states. In contrast, in the $[\mathbf{1x}']^{\bullet-}$ structures, one flurenyl unit shows radical-like magnetism, whereas the other unit is strongly diatropic, implying its predominantly anionic nature. Thus, the NICS maps provide compelling evidence for the distonic character of the $[\mathbf{1x}']^{\bullet-}$ anions. A similar analysis is also valid for the radical cations $[\mathbf{1x}']^{\bullet+}$ and $[\mathbf{2x}']^{\bullet+}$, with the noteworthy exception of the center heterole ring, which is more strongly paratropic than in the corresponding neutral and dicationic states.

The combined experimental and theoretical evidence obtained for difluorenoheteroles can be rationalized in terms of several types of delocalization contributions **I**–**IV**, summarized

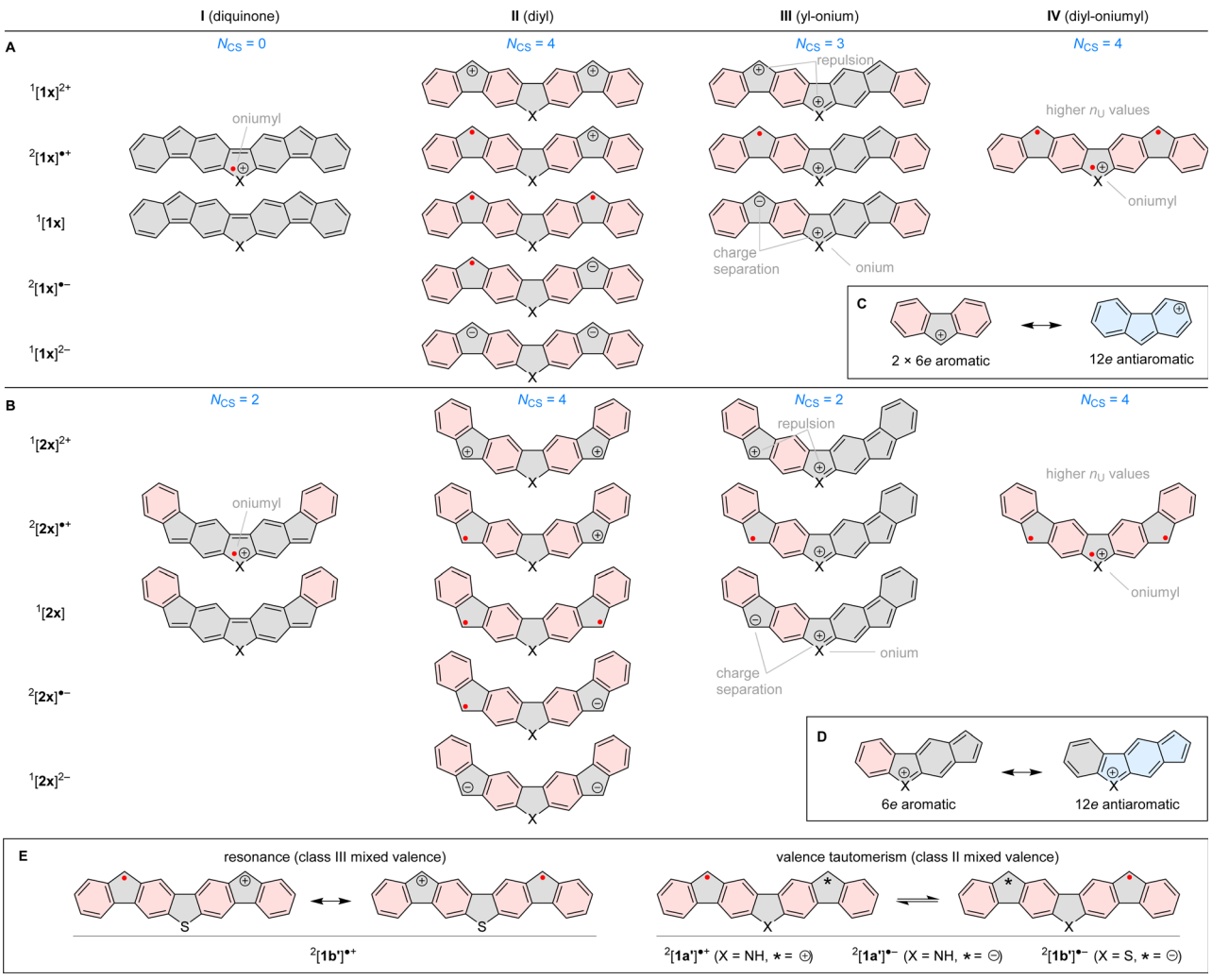

Fig. 6 Conjugation in difluorenoheteroles and their ions. R groups are omitted for clarity. Clar sextets and Hückel-antiaromatic circuits are shaded in red and blue, respectively. (A) Conjugation in **1x** (X = S, NR), (B) conjugation in **2x** (X = S, NR), (C) antiaromaticity the of fluorenyl cation; (D) indacene-like antiaromaticity of benzo[*b*]indeno[5,6-*d*]heterole cations; (E) mixed-valence characters of radical ions, according to CAM calculations.

in Fig. 6A and B. Diquinone contributors **I** can be drawn for both neutral **1x** and **2x**, but they feature low Clar sextet counts N_{CS} (0 and 2, respectively), which makes them less relevant. Analogous structures can formally also be proposed for radical cations by assuming non-octet oniumyl heteroatom sites, but their contribution will likewise be limited. Clar sextet counts are maximized in "diyl" structures **II** ($N_{CS} = 4$), which can be constructed for all oxidation levels of both **1x** and **2x**, and are expected to be the dominant resonance contributors. The diyl structures can also be reinterpreted as consisting of two fluorene units, each at a specific oxidation level (anion, radical, or cation). Ring currents observed in the NICS maps (Fig. 5) are largely consistent with such a formulation, *e.g.* the intrinsic antiaromaticity of the fluorenyl cation (Fig. 6C), is reflected in the magnetic features of the $[\mathbf{1x}']^{2+}$ and $[\mathbf{2x}']^{2+}$ cations.

The presence of heteroatoms in **1x** and **2x** provides additional opportunities for resonance: in the "yl-onium" structures **III**, which are available for all nonnegatively charged states, a formal positive charge is placed on the X site whereas a cationic, radical, or anionic site is located in one of the outer 5-membered rings. Type-**III** contributions are particularly important in radical cations, wherein they do not lead to either charge separation or charge repulsion. Yl-onium structures can be used to construct indacene-like antiaromatic circuits (Fig. 6D), which provide an appealing rationale for the increased paratropicity of heterole rings observed in $[\mathbf{1x}']^{\bullet+}$ and $[\mathbf{2x}']^{\bullet+}$. Finally, "diyl-oniumyl" contributions **IV** can be proposed to explain the elevated n_U^{CAM} values (*ca.* 1.2) determined for $[\mathbf{1x}']^{\bullet+}$ and $[\mathbf{2x}']^{\bullet+}$.

For radical cations and anions of **1x**′ and **2x**′, canonical structures **II** and **III** are inherently unsymmetrical, because of the distonic placement of formal charge and spin sites. This feature may lead to two distinct Robin–Day classes of organic mixed valence:[39,40] class III, with spin and charge uniformly delocalized over the whole ion (C_{2v} symmetry); and class II, characterized by lower symmetry (C_s) and valence tautomerization. CAM geometries and densities (see above) indicate that all **2x** ions should be class-III CT systems, in line with the vibronic structure of their lowest-energy absorption bands. In the **1x** series, the $[\mathbf{1b}']^{\bullet+}$ state is also predicted to belong to class III, and its structure can therefore be described in terms of resonance between the two equivalent type II structures (Fig. 6E). In the remaining ions, $[\mathbf{1a}']^{\bullet+}$, $[\mathbf{1a}']^{\bullet-}$, and $[\mathbf{1b}']^{\bullet-}$, the two type-**II** structures would correspond to valence tautomers.

Conclusions

The two families of difluorenoheteroles described in this work provide a rare opportunity for side-by-side comparison of isomeric structures containing distinct conjugation patterns, thus offering a valuable insight into heteroatom-mediated conjugation effects in organic diradicaloids and their ions. The new fusion pattern introduced herein, based on the X-linked triphenylmethyl dyad (**TD**-X) motif, produces diradicaloids with smaller energy gaps and better redox reversibility than their Chichibabin-like (**CH**) counterparts, making the former systems of interest in organic semiconductor applications. The **TD**-X difluorenoheteroles are less quinoidal than the corresponding **CH** systems, showing instead a stronger involvement of the heteroatom in the overall conjugation. This effect leads to different properties of the **TD**-S and **TD**-NR analogues: quite remarkably, the **TD**-NR diradicaloid features a much larger singlet–triplet gap, showing the ability of the nitrogen bridge to promote antiferromagnetic alignment of spins.

The **TD**-X difluorenoheteroles are particularly notable for the extremely NIR-shifted spectra of their radical cations and anions, a characteristic that can be linked to their mixed-valence character. Unlike their **CH** analogues, which display complete delocalization of spin and charge, leading to fully symmetrical structures, most of the **TD**-X radical ions are predicted to have low-symmetry structures consistent with distonic placement of spin and charge, and corresponding to class-II mixed valence. Efforts to explore this elusive property and correlate it with electronic characteristics of these ions are ongoing in our laboratory.

Data availability

The crystallographic data was provided in Cambridge Structural Database, and the other necessary data of this study have been provided in the ESI.†

Author contributions

B. P. and M. S. designed the experiments and co-wrote the manuscript. B. P., T. K. and M. A. M. performed all the synthetic exeperiments and characterization. T. L. performed X-ray crystallographic analyses. P. J. C. performed electrochemical analyses. C. J. G.-G. performed and analyzed magnetometric measurements. M. S. performed theoretical calculations.

Conflicts of interest

There are no conflicts to declare.

Acknowledgements

Financial support from the National Science Center of Poland (UMO-2019/35/B/ST4/00401 to M. S.) is gratefully acknowledged. Theoretical calculations were performed using the resources provided by the Wrocław Center for Networking and Supercomputing. We thank Prof. Mirosław Czarnecki for help with IR measurements.

Notes and references

1 A. E. Tschitschibabin, *Ber. Dtsch. Chem. Ges.*, 1907, **40**, 1810–1819.
2 L. K. Montgomery, J. C. Huffman, E. A. Jurczak and M. P. Grendze, *J. Am. Chem. Soc.*, 1986, **108**, 6004–6011.
3 X. Chang, M. E. Arnold, R. Blinder, J. Zolg, J. Wischnat, J. van Slageren, F. Jelezko, A. J. C. Kuehne and M. von Delius, *Angew. Chem., Int. Ed.*, 2024, e202404853.

4 M. A. Majewski, P. J. Chmielewski, A. Chien, Y. Hong, T. Lis, M. Witwicki, D. Kim, P. M. Zimmerman and M. Stępień, *Chem. Sci.*, 2019, **10**, 3413–3420.
5 S. Mori, M. Akita, S. Suzuki, M. S. Asano, M. Murata, T. Akiyama, T. Matsumoto, C. Kitamura and S. Kato, *Chem. Commun.*, 2020, **56**, 5881–5884.
6 S. Mori, S. Moles Quintero, N. Tabaka, R. Kishi, R. González Núñez, A. Harbuzaru, R. Ponce Ortiz, J. Marín-Beloqui, S. Suzuki, C. Kitamura, C. J. Gómez-García, Y. Dai, F. Negri, M. Nakano, S. Kato and J. Casado, *Angew. Chem., Int. Ed.*, 2022, **61**, e202206680.
7 X. Lu, T. Y. Gopalakrishna, H. Phan, T. S. Herng, Q. Jiang, C. Liu, G. Li, J. Ding and J. Wu, *Angew. Chem., Int. Ed.*, 2018, **57**, 13052–13056.
8 H. Gregolińska, M. Majewski, P. J. Chmielewski, J. Gregoliński, A. Chien, J. Zhou, Y.-L. Wu, Y. J. Bae, M. R. Wasielewski, P. M. Zimmerman and M. Stępień, *J. Am. Chem. Soc.*, 2018, **140**, 14474–14480.
9 B. Prajapati, D.-K. Dang, P. J. Chmielewski, M. A. Majewski, T. Lis, C. J. Gómez-García, P. M. Zimmerman and M. Stępień, *Angew. Chem., Int. Ed.*, 2021, **60**, 22496–22504.
10 C. K. Frederickson, B. D. Rose and M. M. Haley, *Acc. Chem. Res.*, 2017, **50**, 977–987.
11 Y. Tobe, *Top. Curr. Chem.*, 2018, **376**, 12.
12 T. Kubo, *Chem. Lett.*, 2015, **44**, 111–122.
13 G. E. Rudebusch, J. L. Zafra, K. Jorner, K. Fukuda, J. L. Marshall, I. Arrechea-Marcos, G. L. Espejo, R. Ponce Ortiz, C. J. Gómez-García, L. N. Zakharov, M. Nakano, H. Ottosson, J. Casado and M. M. Haley, *Nat. Chem.*, 2016, **8**, 753–759.
14 C.-C. Lee, C.-I. Chen, C.-T. Fang, P.-Y. Huang, Y.-T. Wu and C.-C. Chueh, *Adv. Funct. Mater.*, 2019, **29**, 1808625.
15 A. C. Valdivia, Y. Dai, F. Rambaldi, J. E. Barker, J. J. Dressler, Z. Zhou, Y. Zhu, Z. Wei, M. A. Petrukhina, M. M. Haley, F. Negri and J. Casado, *Chem.–Eur. J.*, 2023, **29**, e202300388.
16 Y.-C. Hsieh, C.-F. Wu, Y.-T. Chen, C.-T. Fang, C.-S. Wang, C.-H. Li, L.-Y. Chen, M.-J. Cheng, C.-C. Chueh, P.-T. Chou and Y.-T. Wu, *J. Am. Chem. Soc.*, 2018, **140**, 14357–14366.
17 A. Borissov, P. J. Chmielewski, C. J. Gómez García, T. Lis and M. Stępień, *Angew. Chem., Int. Ed.*, 2023, e202309238.
18 T. Y. Gopalakrishna, W. Zeng, X. Lu and J. Wu, *Chem. Commun.*, 2018, **54**, 2186–2199.
19 S. Dong, T. S. Herng, T. Y. Gopalakrishna, H. Phan, Z. L. Lim, P. Hu, R. D. Webster, J. Ding and C. Chi, *Angew. Chem., Int. Ed.*, 2016, **55**, 9316–9320.
20 X. Shi, E. Quintero, S. Lee, L. Jing, T. Seng Herng, B. Zheng, K.-W. Huang, J. T. L. Navarrete, J. Ding, D. Kim, J. Casado and C. Chi, *Chem. Sci.*, 2016, **7**, 3036–3046.
21 X. Shi, T. Y. Gopalakrishna, Q. Wang and C. Chi, *Chem.–Eur. J.*, 2017, **23**, 8525–8531.
22 J. J. Dressler, M. Teraoka, G. L. Espejo, R. Kishi, S. Takamuku, C. J. Gómez-García, L. N. Zakharov, M. Nakano, J. Casado and M. M. Haley, *Nat. Chem.*, 2018, **10**, 1134–1140.
23 J. E. Barker, J. J. Dressler, A. Cárdenas Valdivia, R. Kishi, E. T. Strand, L. N. Zakharov, S. N. MacMillan, C. J. Gómez-García, M. Nakano, J. Casado and M. M. Haley, *J. Am. Chem. Soc.*, 2020, **142**(3), 1548–1555.
24 E. Müller and W. Bunge, *Ber. Dtsch. Chem. Ges. B*, 1936, **69**, 2164–2172.
25 H. S. Jarrett, G. J. Sloan and W. R. Vaughan, *J. Chem. Phys.*, 1956, **25**, 697–701.
26 G. J. Sloan and W. R. Vaughan, *J. Org. Chem.*, 1957, **22**, 750–761.
27 F. Strohbusch and H. Zimmermann, *Tetrahedron Lett.*, 1969, **10**, 1705–1708.
28 L. Viadel, J. Carilla, E. Brillas, A. Labarta and L. Juliá, *J. Mater. Chem.*, 1998, **8**, 1165–1172.
29 A. Rajca, K. Shiraishi, M. Vale, H. Han and S. Rajca, *J. Am. Chem. Soc.*, 2005, **127**, 9014–9020.
30 J. Wang, G. Kim, M. E. Sandoval-Salinas, H. Phan, T. Y. Gopalakrishna, X. Lu, D. Casanova, D. Kim and J. Wu, *Chem. Sci.*, 2018, **9**, 3395–3400.
31 B. Prajapati, M. D. Ambhore, D.-K. Dang, P. J. Chmielewski, T. Lis, C. J. Gómez-García, P. M. Zimmerman and M. Stępień, *Nat. Chem.*, 2023, **15**, 1541–1548.
32 D. Myśliwiec and M. Stępień, *Angew. Chem., Int. Ed.*, 2013, **52**, 1713–1717.
33 E. De Boer and H. Van Willigen, *Prog. Nucl. Magn. Reson. Spectrosc.*, 1967, **2**, 111–161.
34 M. Nakano, *Top. Curr. Chem.*, 2017, **375**, 47.
35 M. Head-Gordon, *Chem. Phys. Lett.*, 2003, **372**, 508–511.
36 M. Parthey and M. Kaupp, *Chem. Soc. Rev.*, 2014, **43**, 5067–5088.
37 K. B. Wiberg, *Tetrahedron*, 1968, **24**, 1083–1096.
38 F. Weinhold and J. E. Carpenter, in *The Structure of Small Molecules and Ions*, ed. R. Naaman and Z. Vager, Springer US, Boston, MA, 1988, pp. 227–236.
39 J. Hankache and O. S. Wenger, *Chem. Rev.*, 2011, **111**, 5138–5178.
40 A. Heckmann and C. Lambert, *Angew. Chem., Int. Ed.*, 2012, **51**, 326–392.